*Structural Durability & Health Monitoring*
DOI:10.32604/sdhm.2020.07663
***Article***



# Fatigue Performance Analysis and Evaluation for Steel Box Girder Based on Structural Health Monitoring System

**Meiling Zhuang[1,2,3], Changqing Miao[1,2,*] and Rongfeng Chen[1,2]**

[1]Key Laboratory of Concrete and Prestressed Concrete Structure of Ministry of Education, Southeast University, Nanjing, 210096, China
[2]School of Civil Engineering, Southeast University, Nanjing, 210096, China
[3]School of Civil, Environmental & Mining Engineering, The University of Adelaide, Adelaide, SA, 5005, Australia
*Corresponding Author: Changqing Miao. Email: chqmiao@seu.edu.cn
Received: 18 June 2019; Accepted: 12 October 2019

**Abstract:** Taizhou Yangtze River Bridge as a long-span suspension bridge, the finite element model (FEM) of it is established using the ANSYS Software. The beam4 element is used to simulate the main beam to establish the "spine beam" model of the Taizhou Yangtze River Bridge. The calculated low-order vibration mode frequency of the FEM is in good agreement with the completion test results. The model can simulate the overall dynamic response of the bridge. Based on the vehicle load survey, the Monte Carlo method is applied to simulate the traffic load flow. Then the overall dynamic response analysis of FEM is carried out. Taking the bending moment of the main beam as the control index, the fatigue sensitive section in the steel box girder of FEM is analyzed. Based on the strain time history data of steel box girder recorded by the structural health monitoring system (SHM), the true stress response of steel box girder under vehicle load is extracted. Taking the cumulative fatigue damage increment as the evaluation index, the fatigue performance evaluation of the steel box girders is conducted based on the collected health monitoring data. The fatigue effect of the beam section near the steel tower, especially the first section of the middle tower, is the key section of the fatigue analysis by health morning system, which is consistent with the calculation results of FEM.

**Keywords:** Steel box girder; fatigue; stress response; Monte Carlo method; structural health monitoring system

## 1 Introduction

Due to the influence of natural factors such as climate and environment, and the increasing traffic volume and the number of overpasses and overpasses, the safety and function of the bridge structure will inevitably degenerate [1-3]. With the rapid development of China's economy, the requirements for transportation capacity are constantly improving, the safety, durability and normal use functions for long-span bridges are paid more and more attention. Hence it is necessary to implement an economically sound maintenance plan and establish a structural health monitoring (SHM) system for large-span bridges [4-6].

Bridge SHM requires simultaneous monitoring of multiple parameters affecting the bridge structure, including environmental, stress, deflection, and dynamic characteristics [7-9]. Health monitoring technology refers to the test components arranged in key sections and key parts of the bridge. The test system is built by computer, and the network is used to remotely and real-time monitor the various reactions of the bridge structure in the operation process.

In general, the SHM systems applied to engineering structures provide an immense amount of recorded data. The data amount depends mainly on the monitoring frequency, data acquisition systems, and the number of sensors [10, 11]. With enhanced realistic deterioration model with the wide application of bridge structure health monitoring technology, the fatigue stress spectrum can be obtained from the strain time history data collected by the SHM system.

In recent years, scholars at home and abroad have gradually realized the fatigue problem of orthotropic steel bridge decks. Zhang et al. [12, 13] systematically sorted out the fatigue problem, fatigue characteristics and evaluation method of the current orthotropic steel bridge deck, and analyzed the new structure of the orthotropic steel bridge deck. Connor et al. [14] discussed the fatigue problem of the OSDs from the aspects of manufacturing, testing, inspection, evaluation and maintenance. In order to accurately predict the fatigue damage of steel box girder and establish a perfect anti-fatigue design analysis method, many scholars have carried out plenty of research work [15-19].

Above all, with the wide application of bridge structure health monitoring technology, the fatigue stress spectrum can be obtained from the strain time history data collected by the SHM system. Compared with the stress spectrum calculated according to the norm or statistical vehicle load the actual working state of the bridge structure is more truly and accurately reflected, and the accuracy and reliability of the structural fatigue life assessment are realized [20]. Therefore, based on the strain time history data recorded by the Taizhou Bridge Health Monitoring System, this paper studies the fatigue stress characteristics of steel box girder under the action of the vehicle load and analyzes the fatigue critical section of the steel box girder, the fatigue performance obtained by the SHM will be compared with the calculation results using the ANSYS software. Authors are encouraged to use the Microsoft Word template when preparing the final version of their manuscripts. Authors may elect to submit two versions of their manuscript, one for the printed version of the journal, and the other for the on-line version. Illustrations in color are allowed only in the on-line version of the journal.

## 2 Finite Element Model

### *2.1 Engineering Background*

The Taizhou Yangtze River Bridge is located in the middle section of the Yangtze River in Jiangsu Province. It is connected to Taizhou in the north and Zhenjiang and Changzhou in the south. The total length of the route is 62 Km. The main bridge of Taizhou Bridge is a three-tower and two-span continuous stiffening box -girder system suspension bridge, shown in Fig. 1. The side tower is a concrete structure. The materials of the middle tower and stiffening beam are steels. The span ratio of the main span is 1/9,

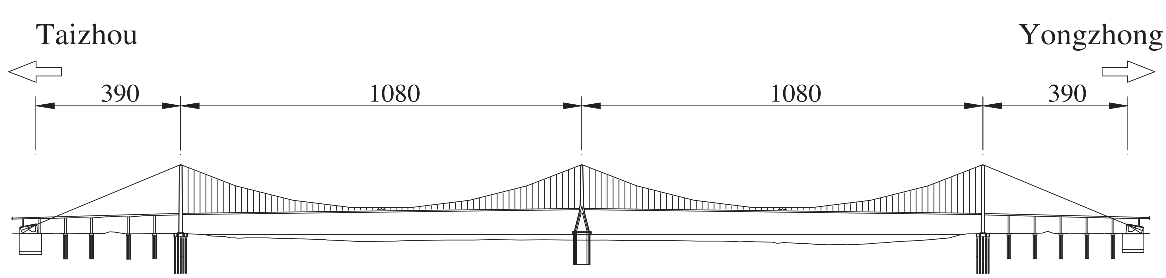


**Figure 1:** The overall Layout of Taizhou Yangtze River Bridge (unit: m)

and the span of the main cable is 390 m + 2 × 1080 m + 390 m. The vertical connection between the main beam and the middle tower is selected such that the main beam does not have a vertical rigid constraint at the middle tower, but a vertical limit stop is supported, a longitudinal elastic constraint is provided, and a wind-resistant support is laterally disposed. A longitudinal damper is arranged at the side tower to connect the main beam and main tower, and a vertical tension and compression support is arranged to restrain the vertical displacement of the main beam end, and the joint of the upper and lower vertical supports restrains the torsion of the beam end; A lateral wind-resistant bearing is provided at the beam end. The main beam of Taizhou Bridge adopts flat steel box girder structure, the beam height is 3.5 m, the full width (including wind nozzle) is 39.10 m, and the aspect ratio is 1:11.17. The steel box girder structure is made of Q345qD and Q235qD steel, all welded. A steel box girder is provided with a diaphragm at 3.2 m.

### *2.2 Finite Element Model of Taizhou Yangtze River Bridge*

The main beam of the Taizhou Yangtze River Bridge is simulated by the "spine beam" of the single main beam using the ANSYS software. The model established can truly reflects the force of the structure. And the change of the vertical curve of the stiffening beam is considered.

#### *2.2.1 The Simulation for the Deck System*

Full welded streamlined flat steel box girder structure is applied in the main beam of the Taizhou Yangtze River Bridge. The orthotropic steel bridge decks are used in the steel box-girders. The typical box-girder segment of Taizhou Yangtze River Bridge is shown in Fig. 2. The girder, including wind fairing, is 39.1 mm × 3.5 mm, the roof width is 36.7 m, the floor width is 21.25 m, the transverse spacing of straight webs is 33.2 m, the spacing of transverse diaphragm is 3.2 m, and the spacing of U-ribs is 600 mm. The outside of the middle lane roof within the range of 6 m is 16 mm thick, and the U-rib is 8 mm thick, the remaining area roof is 14 mm thick, and the U-rib is 6 mm thick. The main structure of the box girder is made from Q345-D steel. The main parameters are roof thickness ($t_d$), U-rib thickness ($t$), U-rib height ($H$) and U-rib opening size ($a$), respectively. The values of the parameters are as following: On the ordinary lane, $t_{d1}$ = 14 mm, $t_1$ = 6 mm, $H_1$ = 280 mm, $a_1$ = 300 mm. On the heavy truck lane, $t_{d2}$ = 16 mm, $t_2$ = 8 mm, $H_2$ = 280 mm, $a_2$ = 300.2 mm.

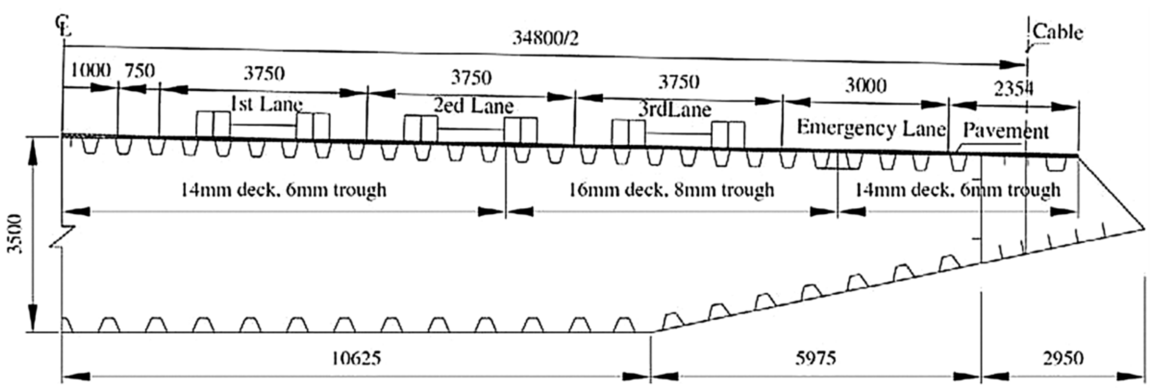


**Figure 2:** Local cross section diagram of the typical box-girder segment

For the simulation of the deck system, the following equivalent principles should be followed: (1) The cross-sectional area is equal; (2) The equivalence of structural stiffness, including the equivalent of transverse, vertical, torsional stiffness and constrained torsional stiffness; (3) Equivalent of spatial distribution of mass system.

The main beam is simulated by the Beam4 element. The quality of the beam element shall be the mass of the deck system, in addition to the quality of the stiffening beam itself, as well as the quality of the transverse baffles, deck pavements, railings, sidewalks, etc. For the equivalent of the mass distribution, the translational mass and the rotational mass of the bridge deck are equivalent by setting the mass unit (Mass21 unit). For translational mass calculations, all masses of the unit length deck system can be divided by the cross-sectional area of the stiffening beam to obtain a converted density as the mass density of the beam elements in all directions. For the calculation of the rotational mass, the main beam, the bridge deck pavement, the railing, etc. can be calculated respectively for the moment of inertia around the longitudinal axis of the bridge, and then accumulated and distributed to each mass element.

*2.2.2 Cable System Simulation*

The main cable and the suspension rod of the suspension bridge are simulated by the Link10 element. The main cable is separated according to the lifting point of the suspension rod, and the single suspension rod is used as an element. The main cable will have a certain sag under its own weight, and the Link10 unit itself cannot automatically consider this sag effect. In order to consider this effect, the bridge is modified in the modeling process by using the Ernst formula (Eq. (1)) to adjust the elastic modulus of the material.

$$E_{eq} = \frac{E}{1 + \frac{(\gamma l)^2}{12\sigma^3}} \tag{1}$$

The suspension bridge is a nonlinear large-displacement cable structure system. Under the action of external load, the main cable structure will form a certain tension. The existence of this tension makes the cable's resistance to deformation under external load enhanced. In the state of bridge formation, due to the self-weight of the dead load, the main cable will form a strong pulling force. Therefore, this gravity stiffness effect should be considered in the calculation, which can be achieved by setting the initial strain of the rod unit. The initial strain can be obtained by using the suspension bridge calculation theory under the dead state of the bridge.

*2.2.3 The Tower Simulation*

The middle tower of the Taizhou Yangtze River Bridge is a vertical herringbone steel tower with a gantry frame structure in the horizontal direction; the two side towers are reinforced concrete structures, and the tower columns are single-box multi-chamber sections. When simulating the tower, it can be simplified into a three-dimensional solid beam element, which is simulated by Beam4 element. The moment of inertia and torsional moment of inertia are still the actual size of the box section.

*2.2.4 Boundary Conditions*

Column: Consolidation at the bottom of the tower.

Main box-girder: The main beam can be vertically rotated, laterally rotated and horizontally moved at the crossbeams of the two towers, and the main direction is constrained by other directions; The main box girder can be vertically moved, vertically rotated, laterally rotated and twisted and rotated at the middle tower beam. The lateral movement freedom adopts the master-slave constraint, and the longitudinal horizontal movement freedom is restrained by the longitudinal elastic cable.

Main cable: The main cable is consolidated at the anchorage point, and the main cable and the pylon are consolidated at the top of the bridge tower. The model of the Taizhou Yangtze River Bridge is shown in Fig. 3.

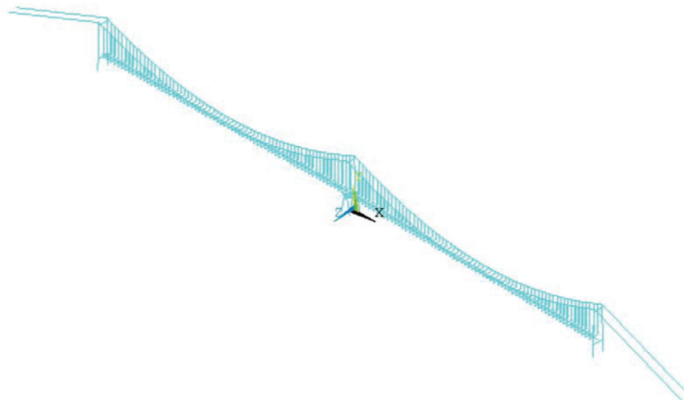

**Figure 3:** The finite element model

### *2.3 Dynamic Characteristics*

In order to consider the influence of large deformation effect and gravity stiffness effect in finite element calculation analysis, the modal analysis of suspension bridge is carried out by using prestressed analysis method. The solution process is as follows: (1) Solving the nonlinear static equilibrium position; (2) Performing structural static analysis with cable tension at the equilibrium position sought; (3) Modal analysis with cable tension.

The self-vibration characteristics of the Taizhou Bridge calculated by the above analysis method are compared with the test results of the self-vibration characteristics of the completion test, as shown in Tab. 1. It can be seen from Tab. 1 that the low-order vibration mode frequency obtained by the modal analysis method with the prestressed structure agrees well with the completion test results, indicating that the established "spine beam" model can accurately simulate the overall dynamics response of the suspension bridge response.

**Table 1:** Dynamic characteristics parameters for the main beam

| Number | Mode | Finite element simulation | Completion test | Rate of change (%) |
|---|---|---|---|---|
| 1 | First-order anti-symmetric lateral bending | 0.08443 | 0.0915 | 7.7 |
| 2 | First-order anti-symmetric vertical bending | 0.08491 | 0.0808 | −5.1 |
| 3 | First-order positive symmetric lateral bending | 0.10678 | 0.1053 | −1.4 |
| 4 | Second-order anti-symmetric vertical bending | 0.11435 | 0.1190 | 3.9 |
| 5 | Second-order positive symmetric vertical bending | 0.11719 | 0.1202 | 2.5 |

The fundamental frequency is 0.08443 Hz, which has a long structural period and has obvious large-span flexible structural features. The first-order mode is dominated by the anti-symmetric lateral bending, rather than the first-order positive symmetric vertical bending of the conventional long-span suspension bridge with two towers. Because the restraining action of the middle tower makes the main beam lateral bending mode forms an inflection point at the middle tower. The 1st-order anti-symmetric side-bend mode of the Taizhou Bridge is equivalent to the 1st-order positive symmetric lateral bending mode of the single-span suspension bridge with two towers in any of its main spans.

## 3 Monte Carlo Method for Simulating Traffic Load Flow

The Jiangyin River Bridge is the most important bridge in the main highway of China from the Tongjiang to Sanya Expressway. It is the throat part of the traffic artery between the north and south of the country. As a bridge to ease the traffic pressure in the east, the traffic flow characteristics for Taizhou Yangtze River Bridge are similar with those for the Jiangyin River Bridge. Therefore, the traffic flow survey data of the Jiangyin Bridge can be approximated for the Taizhou Yangtze River Bridge, representing the traffic flow characteristics of the Taizhou Yangtze River Bridge after it is opened. The vehicle traffic flow, vehicle type, vehicle weight and axle spacing are statistically analyzed, and a probability and statistical model is established. The Monte Carlo method [21] is also known as a stochastic simulation method and is sometimes referred to as a random sampling technique or a statistical test method. The Monte Carlo method is used to simulate the traffic load flow.

### *3.1 Basic Principle of Monte Carlo Method*

Monte Carlo methods a class of computational algorithms that rely on repeated random sampling to compute their results. Monte Carlo methods are ofen used when simulating physical and mathematical systems. Because of their reliance on repeated computation and random or pseudo–random numbers, Monte Carlo methods are most suited to calculation by a computer.

The main idea behind this method is that the results are computed based on repeated random sampling and statistical analysis. The Monte Carlo simulation is, in fact, random experimentations, in the case that, the results of these experiments are not well known. Monte Carlo simulations are typically characterized by many unknown parameters, many of which are difficult to obtain experimentally. Monte Carlo simulation methods do not always require truly random numbers to be useful (although, for some applications such as primality testing, unpredictability is vital). Many of the most useful techniques use deterministic, pseudorandom sequences, making it easy to test and re-run simulations. The only quality usually necessary to make good simulations is for the pseudo-random sequence to appear "random enough" in a certain sense.

What this means depends on the application, but typically they should pass a series of statistical tests. Testing that the numbers are uniformly distributed or follow another desired distribution when a large enough number of elements of the sequence are considered is one of the simplest and most common ones. Weak correlations between successive samples are also often desirable/necessary.

### *3.2 Vehicle Load Parameter Probability Model*

The amount of data in the traffic flow fitting analysis is generally large, and if too many factors are considered, it will cause a huge computational load on the computer. The vehicle load problem is simulated by three units of vehicle model, vehicle weight and vehicle spacing. The following gives the formula parameters of the vehicle flow:

#### *3.2.1 Vehicle Type*

Under normal circumstances, the proportion of different models does not satisfy the uniform distribution. In order to more accurately fit the traffic flow, firstly, according to the existing survey results, the distribution function is fitted, and then the distribution function is fitted by Monte Carlo method.

#### *3.2.2 Vehicle Weight*

The vehicle weight data satisfies the extreme value I distribution, and its distribution function is:

$$F(x) = \exp\{-\exp[-a(x-u)]\} \tag{2}$$

In the formula: $a$, $u$ - extreme value I type distribution parameters;

$x$—a random number that satisfies the extreme value I distribution; Available from (2):

$$x = \frac{1}{a}\ln\left[\ln\left(\frac{1}{r}\right)\right]^{-1} + u \tag{3}$$

In the formula: $r$ - a uniformly distributed random number over the interval (0, 1).

The uniformly distributed random number sequence in the (0, 1) interval is converted into an extreme value I type random number sequence by Eq. (3).

*3.2.3 Vehicle Distance*

When a certain section of the bridge is only affected by the single load of the vehicle or the vehicle load on the same section is a non-negative stationary stochastic process, the single-lane vehicle operating state vehicle load stochastic process can be expressed by the Poisson process. When the random process of vehicle load is filtered through the composite Poisson process, the time interval $t$ of the vehicle obeys the exponential distribution, and the probability density distribution function is:

$$F(t) = \begin{cases} 0 & t < 0 \\ 1 - e^{-\lambda t} & t \geq 0 \end{cases} \tag{4}$$

In the formula: parameter $\lambda > 0, \lambda = 1/\mu_t, \mu_t$ is the mean of $t$.

The probability expression of the time interval $t$ is

$$t = -\lambda^{-1}\ln[1 - F(t)] = -\mu_t \ln[1 - F(t)] \tag{5}$$

Assuming that $\xi = F(t)$ is a uniformly distributed random variable in the interval (0, 1), a random sample of the time interval $t$ obeying the exponential distribution can be obtained by:

$$t = -\lambda^{-1}\ln(1 - \xi) = -\mu_t \ln(1 - \xi) \tag{6}$$

Assuming the vehicle speed is $V$, the vehicle spacing $x$ expression can be:

$$x = -V\mu_t \ln(1 - \xi) \tag{7}$$

### *3.3 Vehicle Load Statistics and Simulation*

*3.3.1 Number of Vehicles and Vehicles*

The two-way daily average traffic flow from 2002 to 2007 is shown in Fig. 4. It can be seen that the traffic flow increased from 2002 to 2007 year by year. In 2002, the average daily traffic volume was 20,000 vehicles. In 2007, the average daily traffic volume reached 39,568 vehicles, with an average growth rate of about 6%. Considering the growth of traffic flow in the future, the daily average traffic volume of Taizhou Bridge will change. Assuming that the average daily traffic volume of the Taizhou Yangtze River Bridge is 50,000 vehicles, the daily traffic volume per lane is 8.

The vehicle type is classified according to the number of the vehicle axles, and it is divided into two types: two-axle and nine-axle, and the two-axle is subdivided into three or less and three or more. Therefore the models can be divided into 9 types, shown in Tab. 2. Fig. 5 shows the proportion of various types of vehicles from June 2006 to June 2007. It can be seen that the three types of vehicles, Model 2, Model 4, and Model 5 account for 84.5% of the traffic volume, which is the main vehicle type on the bridge.

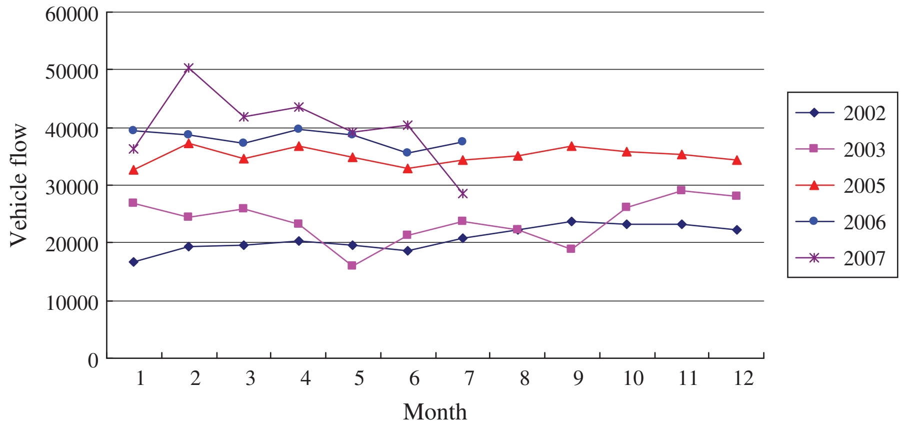


**Figure 4:** Daily average traffic flow statistics

**Table 2:** Classification of vehicle types

| Vehicle types | Number of axes | Vehicle weight |
|---|---|---|
| Vehicle-1 | 2 | $\leq$ 3t |
| Vehicle-2 | 2 | > 3t |
| Vehicle-3 | 3 | |
| Vehicle-4 | 4 | |
| Vehicle-5 | 5 | |
| Vehicle-6 | 6 | |
| Vehicle-7 | 7 | |
| Vehicle-8 | 8 | |
| Vehicle-9 | 9 | |

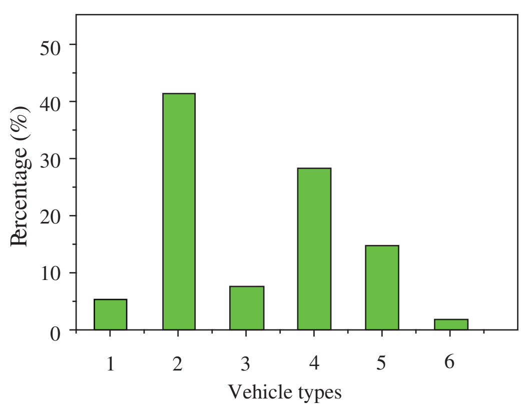


**Figure 5:** Flow ratio of each vehicle type

Vechicles 7, 8 and 9 are rare in statistics. In order to simplify the calculation, Vehicles 7, 8, and 9 are not simulated. According to the proportion of the models surveyed, the proportion of the fitted models is shown in Fig. 6.

#### *3.3.2 Statistical Analysis and Simulation of Vehicle Weights of Different Vehicle types*

The vehicle statistics from June 2006 to June 2007 are analyzed. Tab. 3 shows the distribution of vehicle weights for different vehicle types. According to the statistical characteristics of the vehicle weight, the vehicle weight distribution of the first six models fitted according to the extreme value-I distribution are shown in Fig. 7.

#### *3.3.3 Vehicle Distance Simulation*

After comprehensive survey data, the vehicle speed is approximately 100 km/h. The average time interval of the vehicle is 17 seconds, that is, $\mu t = 0.7$ s and $V = 27.78$ m/s in formula (7).

The corresponding vehicle spacing samples can be obtained by the Monte Carlo method. The results of vehicle spacing fitting and vehicle spacing cumulative probability distribution are shown in Figs. 8 and 9, respectively.

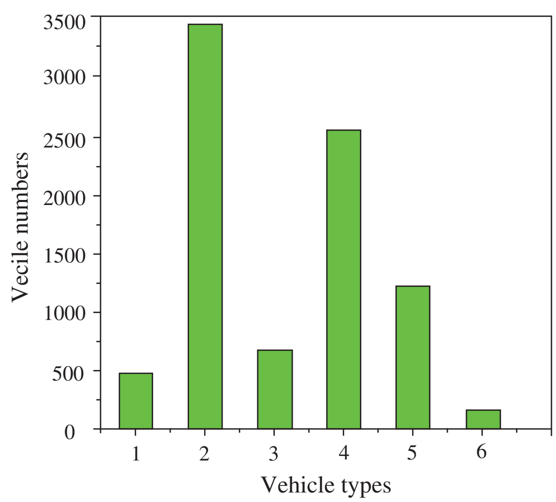


**Figure 6:** Distribution of each vehicle type fitted by statistical results

**Table 3:** Statistical characteristics of vehicle weight

| Vehicle types | Average vehicle weight | Vehicle weight variance |
|---|---|---|
| Vehicle-1 | 2.28 | 0.54 |
| Vehicle-2 | 8.89 | 4.92 |
| Vehicle-3 | 21.54 | 6.93 |
| Vehicle-4 | 32.25 | 8.85 |
| Vehicle-5 | 39.87 | 10.42 |
| Vehicle-6 | 38.71 | 12.87 |

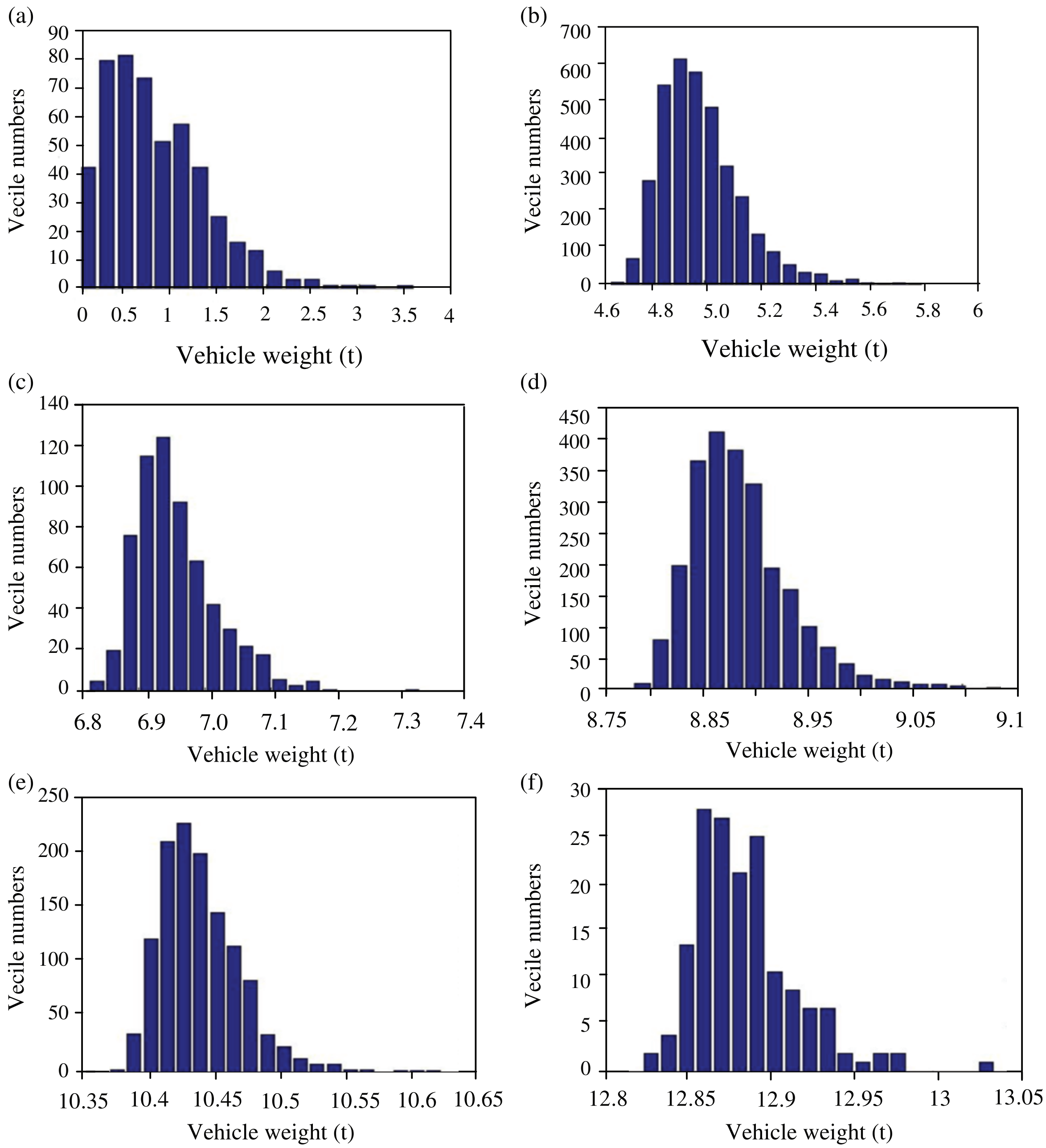


**Figure 7:** Fitting results for different vehicle types. (a) Vehicle-1 weight distribution, (b) Vehicle-2 weight distribution, (c) Vehicle-3 weight distribution, (d) Vehicle-4 weight distribution, (e) Vehicle-5 weight distribution, and (f) Vehicle-6 weight distribution

### *3.4 Monte Carlo Method to Generate Random Traffic*

In the process of generating random traffic, the three parameters of vehicle type, vehicle weight and vehicle spacing are regarded as independent unrelated and variables. The Monte Carlo method is used to generate the simulated traffic flow. The specific process is as following:

1. Generate a corresponding vehicle type code by uniformly distributing random numbers.

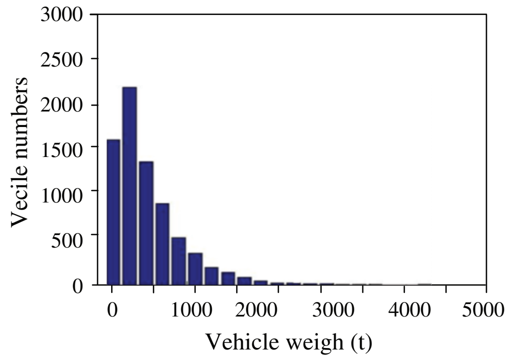


**Figure 8:** The results of vehicle spacing fitting

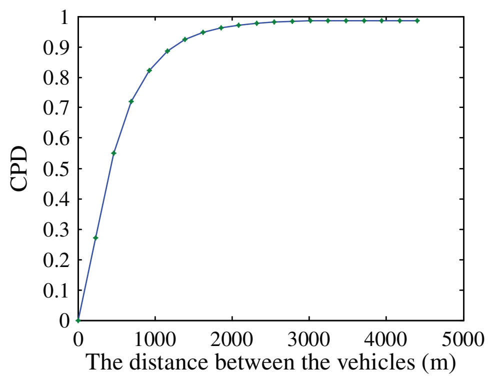


**Figure 9:** Vehicle spacing cumulative probability distribution

2. Generating a vehicle type data sequence according to the number of vehicles.
3. According to different vehicle types, input the front and rear axle bearing ratios. wheelbases and vehicle weight parameters of different vehicle types, and convert the uniformly distributed random numbers into extreme value I-type random variables through function relations to obtain vehicle weight data.
4. Calculate the car spacing by transforming the uniformly distributed random number into a lognormal distribution random variable through a functional relationship.
5. Mix the vehicle weight data with the vehicle spacing data and write the data file.

### *3.5 Dynamic Response Analysis Under Random Traffic*

The generated random traffic flow is loaded on the FEM. Under the vehicle load, different parts of the main beam will produce different degrees of dynamic response. In order to determine the stress-sensitive beam section of the main beam under the action of random traffic flow, the displacement and bending moment dynamic response of the main beam are analyzed. The reference position of the coordinate system and the position of the main beam are divided, shown in Fig. 10, where L(R)-20 indicates the position of the first boom of the left (right) middle tower.

#### *3.5.1 Displacement Response Analysis of FEM*

The displacement response of the main beam at each control section under simulated traffic flow is shown in Fig. 11. The curve is calculated with a time duration of 500 seconds and a sampling frequency of 10 Hz. It can be seen that under the action of random traffic flow, the maximum vertical displacement

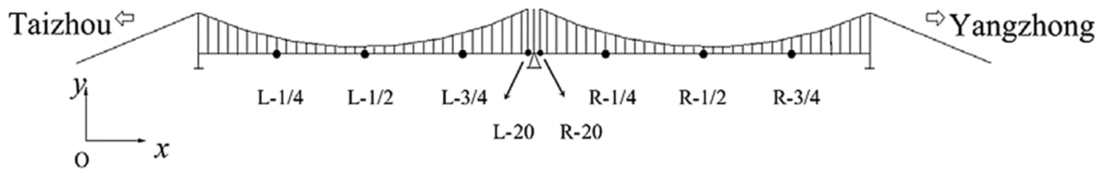


**Figure 10:** Reference position of the coordinate system and the main beam position division

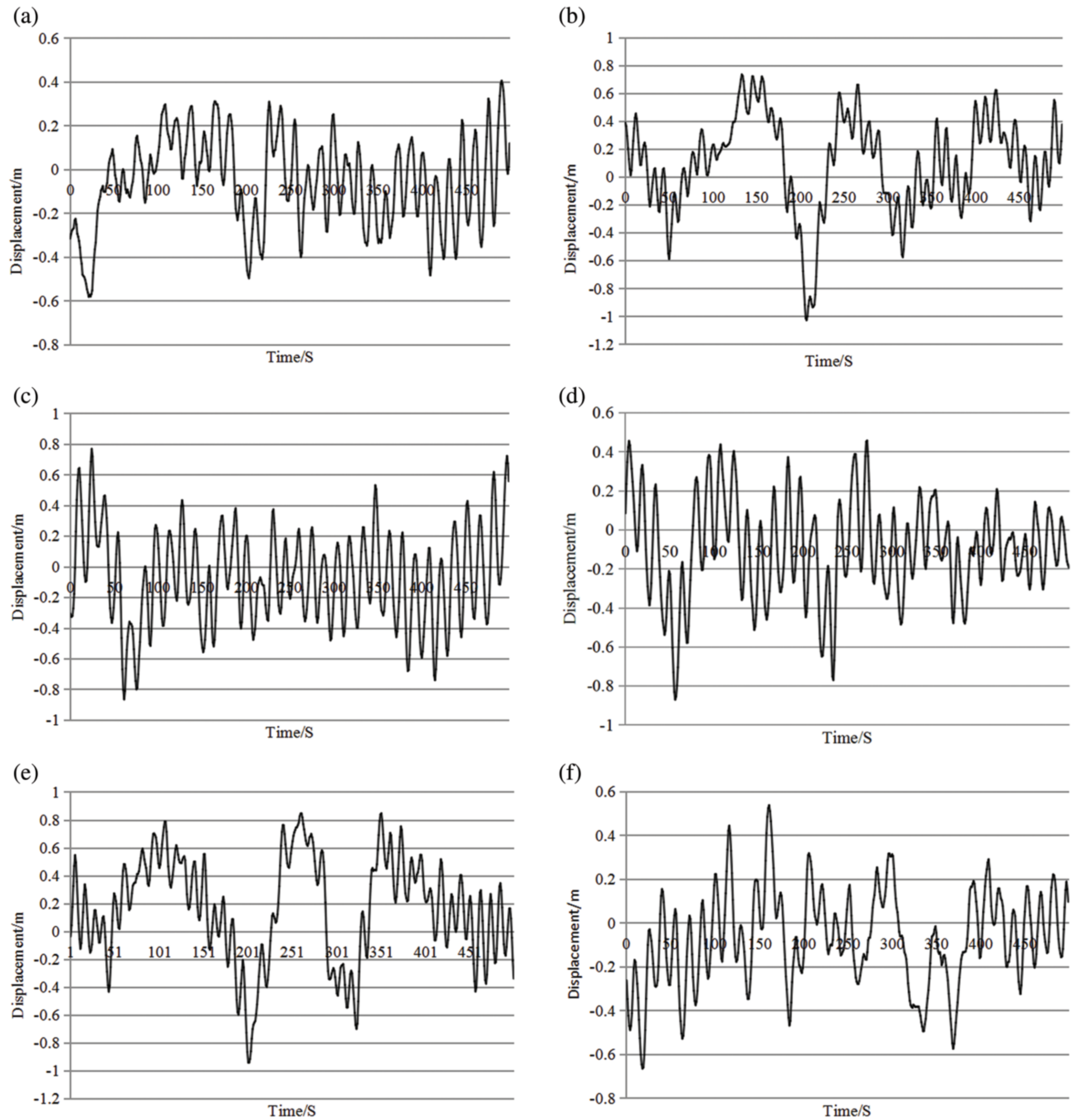


**Figure 11:** The displacement response at each control section. (a) L-1/4, (b) L-1/2, (c) L-3/4, (d) R-1/4, (e) R-1/2, and (f) R-3/4

values of the left and right sides of the steel box girder are 1.01 m and 0.95 m, respectively. The displacement values are close to each other. The maximum vertical displacement values at L-1/4 and R-1/4 are 0.58 m and 0.87 m respectively; the maximum vertical displacement values at L3/4 and R-3/4 are 0.86 m and 0.65 m respectively. The calculation results show that the vertical displacement response of the steel box girder at the corresponding section position is almost the same, but the vertical displacement response of the same main span at the corresponding section position is different, and the displacement near the section of the steel tower is different. The displacement response of the section near the steel tower is larger than that of the section near the side tower due to the different constraints of the middle flexible steel tower to the main beam.

*3.5.2 Analysis of Bending Moment Response of FEM*

The main force-receiving members of the suspension bridge are the main cable and the pylon. The main beam is mainly subjected to bend, which can be equivalent to the bending member. At the same time, the change of bending moment of steel box girder during dynamic analysis is the main factor affecting the stress amplitude. Therefore, this section analyzes the fatigue sensitive parts of steel box girder with the main beam bending moment as the evaluation standard.

Fig. 12 shows the time-reaction curve of the moment response at the section of the main beam. The calculation time is 250 seconds and the sampling frequency is 10 Hz. It can be seen from that under the action of random traffic, the bending moment of the main beam is constantly changing and consists of several cycles.

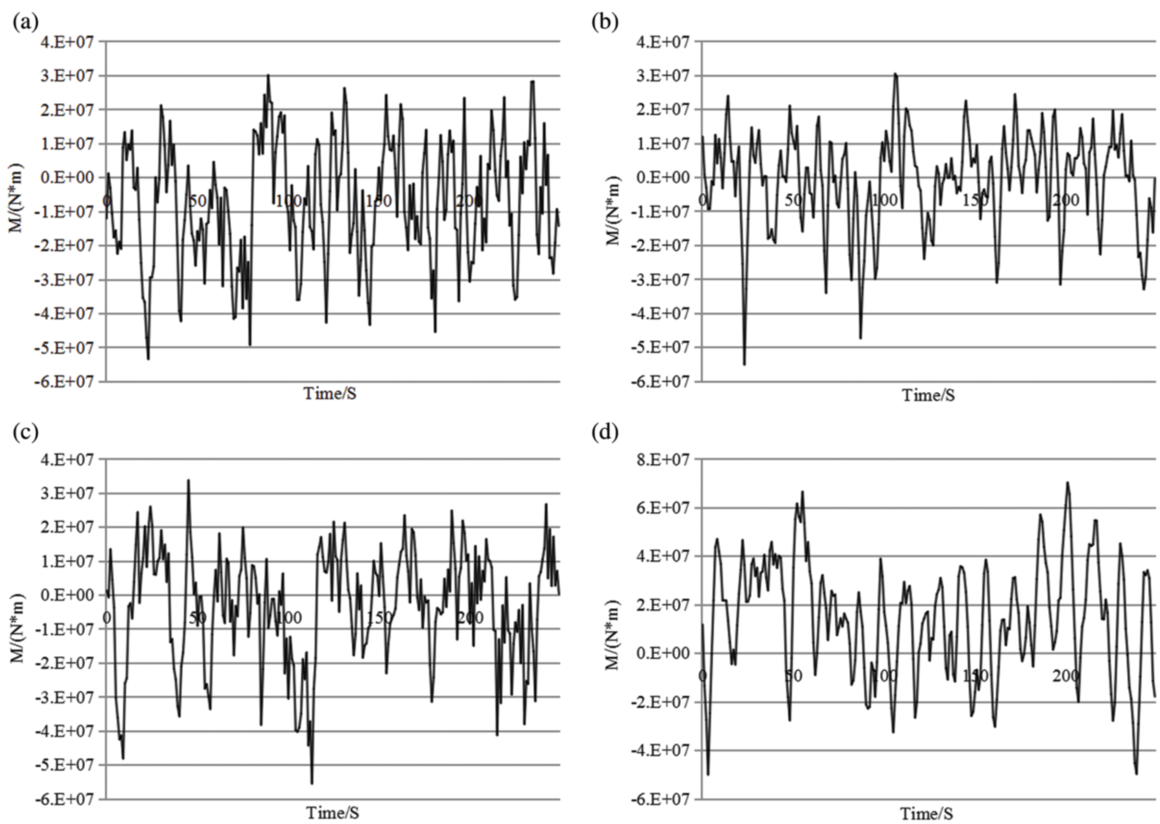


**Figure 12:** The bending moment response at each control section. (a) L-1/4, (b) L-1/2, (c) at L-3/4, and (d) The first boom position on the left side

The variation range of the bending moment at each control section is shown in Tab. 4. It can be seen from that the bending moment of the main beam is the largest at the cross-section position of the first suspension point around the middle tower, where the positive bending moment of the main beam is much larger than the other sections, and the bending moment range at eight points varies approximately the same.

The peak envelope of the bending moment response of Taizhou Bridge under random traffic flow is shown in Fig. 13. It can be seen from that the peak value of the bending moment response of the steel box girder on both sides of the Taizhou Yangtze River Bridge is approximately the same at the corresponding section position. The maximum bending moment response value of the main beam is 7.02 × 107 N*m, which is located on the left side of the middle tower. At the position of the root boom, the minimum bending moment response of the main beam is −6.15 × 107 N*m, which is located at the middle tower position.

**Table 4:** Variation range of bending moment of each control section of main beam

| Control section | Bending moment variation range | | Control section | Bending moment variation range | |
|---|---|---|---|---|---|
| | MAX | MIN | | MAX | MIN |
| L-1/8 | 3.19 | −5.37 | R-20 | 6.78 | −5.00 |
| L-2/8 | 3.35 | −5.38 | R-1/8 | 3.39 | −5.31 |
| L-3/8 | 3.15 | −5.72 | R-2/8 | 3.05 | −5.90 |
| L-4/8 | 3.38 | −5.28 | R-3/8 | 3.40 | −5.58 |
| L-5/8 | 3.01 | −5.06 | R-4/8 | 3.23 | −5.39 |
| L-6/8 | 3.33 | −5.58 | R-5/8 | 3.13 | −5.32 |
| L-7/8 | 3.64 | −5.78 | R-6/8 | 3.02 | −5.09 |
| L-20 | 7.00 | −5.02 | R-7/8 | 2.88 | −5.41 |
| 中塔 | 5.94 | −6.15 | | | |

**Note:** L indicates the left span, R indicates the right span, X/8 indicates the position of the eight points, and L(R)-20 indicates the position of the first boom to the left (right) of the middle tower.

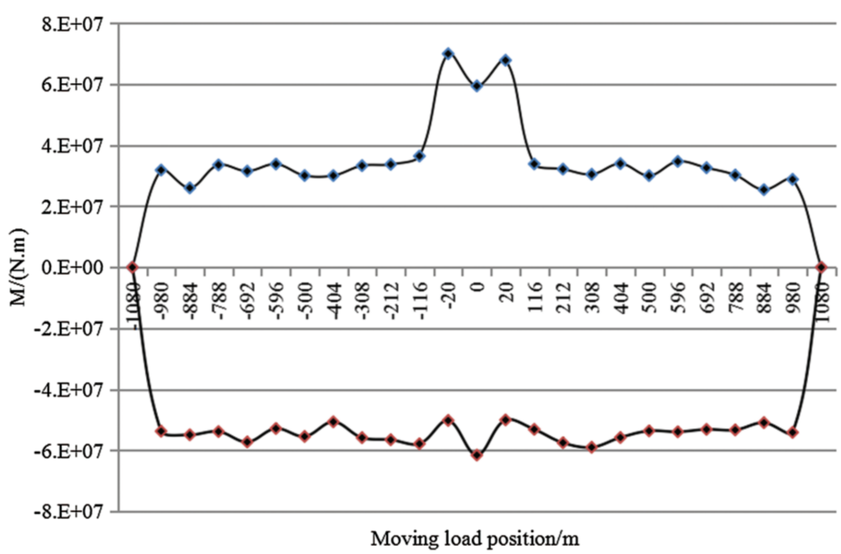


**Figure 13:** Peak envelope diagram of the bending moment response

The bending moment variation range of the main beam near the middle tower is larger than that of other sections, especially in the range of the bending moment of the first boom position around the middle tower due to the different constraints of the tower on the main beam in the flexible steel.

The change of the bending moment of the steel box girder directly leads to the change of the stress, which is the main reason for the stress amplitude. The fatigue of the steel box girder is not only related to the stress amplitude, but also to the number of stress cycles. In order to truly reflect the stress variation of steel box girder and quantify the degree of bending moment vibration at each control section, the bending moment comprehensive coefficient $M_R$ is proposed in this paper.

First, the index m with the dimension is calculated according to the formula (8):

$$m = \sum |A_{i+1} - A_i|/t \tag{8}$$

where $A_i$ is the $i$-th extreme value in the moment history curve, $A_{i+}1$ is the ($i$+1)-th extreme, and $t$ is time.

*m* reflects the degree of the bending moment change per unit time, the dimension is KN*m/s, which is reasonable consideration of the influence of each amplitude, less affected by the irregularity of the response curve.

In order to eliminate the influence of the dimension, the *m* is processed by a standardized method, that is, the bending moment synthesis coefficient M is obtained. The standardization formula is:

$$M_{Ri} = (m_i - \overline{m})/s \tag{9}$$

In formula (9),

$$\overline{m} = \frac{1}{n}\sum_{i=1}^{n} m_i \tag{10}$$

$$s = \sqrt{\frac{1}{n-1}\sum_{i=1}^{n}(m_i - \overline{m})^2} \tag{11}$$

The numerical sequence of the time-history curve of the bending moment response of the main beam is derived, and the bending moment synthesis coefficient is obtained according to the above process, shown in Fig. 14. It can be seen from that the composite coefficient of the bending moment of the main beam at the side tower is the smallest, which is caused by the simple constraint of the steel box girder at the side tower.

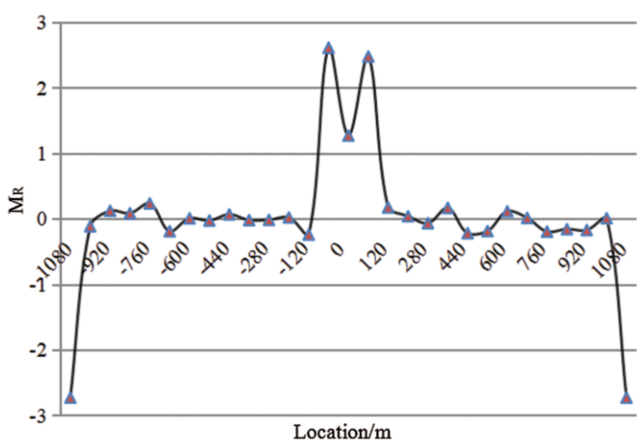


**Figure 14:** Distribution of bending moment synthesis coefficient

The composite moment coefficient of the main beam near the middle tower is the largest, which is caused by the different constraints of the middle flexible steel tower to the main beam. The bending moment synthesis coefficients of other beam sections are basically the same. The bending moment comprehensive coefficient reflects the severity of the bending moment variation, which indirectly reflects the degree of stress variation of the steel box girder. That is to say, the stress variation of the beam section near the steel tower is more severe, and the fatigue effect is more obvious. Therefore, the beam section near the steel tower, especially the beam section at the first boom position around the middle tower is the key section of the fatigue analysis.

### *3.6 Health Monitoring System of Taizhou Yangtze River Bridge*

The Taizhou Yangtze River Bridge Health Monitoring System consists of a sensor subsystem, a data acquisition and transmission subsystem, a data processing and control subsystem.

The sensor subsystem mainly consists of various sensors and transmission cables for test parameters such as bridge natural environment, vehicle load and speed, temperature and humidity, strain, vibration and deflection. It mainly completes the transmission and transmission functions of the bridge structure environmental state and load signals as well as various dynamic and static response signals.

The data acquisition and transmission subsystem of Taizhou Yantze River Bridge adopts the combination of centralized acquisition and distributed acquisition based on board. For the first time, the combination of wired acquisition transmission and wireless acquisition transmission is adopted. The main method of the wired acquisition system is to set up a workstation at the appropriate part of the bridge, select the industrial computer as the collection terminal, introduce various types of sensor signals into the collection terminal through the wires, and use the relevant software for data acquisition and processing. The wireless acquisition system adopts the distributed network and network node peer-to-peer working mode, and has the characteristics of convenient installation and strong mobility, which can effectively compensate for the lack of flexibility and short transmission distance of the wired collection system.

The data processing and control subsystem is the core of the Taizhou Yangtze River Bridge SHM system. The main function is to process and analyze the data transmitted by the acquisition system, including data preprocessing, secondary processing, data storage and data display and other data management control.

The monitoring project of the large-span bridge SHM system usually includes three aspects: bridge working environment monitoring, bridge structure condition monitoring and structural response behavior monitoring. According to the structural characteristics of the three-tower and two-span suspension bridge, the structural health monitoring system of Taizhou Yangtze River Bridge will focus on monitoring the middle tower, taking into account the main beam and the main cable, and through various technical means, the overall linear shape, stress strain, vibration and wind load of the bridge structure. Corresponding sensors mainly include GPS systems, strain sensors, acceleration sensors, anemometers, temperature sensors, humidity sensors, and the like. The types and quantities of sensors are shown in Tab. 5.

**Table 5:** Sensor types and quantity

| Name | Wind speed and direction instrument | Air temperature and humidity sensor | GPS system | | Accelerometer | | Fiber optic cable sensor | |
|---|---|---|---|---|---|---|---|---|
| | | | Reference station | Receiving station | Two-way | Three-way | strain | temperature |
| Number | 1 | 1 | 1 | 11 | 39 | 12 | 168 | 42 |
| Total | 275 | | | | | | | |

Based on the strain and temperature time history data recorded by the fiber optic cable sensor on the box girder structure, the fatigue stress characteristics of the steel box girder under the operational load is analyzed. Therefore, the fiber optic cable sensor disposed on the steel box girder needs to be introduced in detail.

The layout of the fiber grating sensor on the steel box girder is shown in Fig. 15. It can be seen that the sensor is arranged on 11 sections of the main beam, where the Sections 1 and 11 are located at the side tower and the Section 6 is located at the middle tower. 2, 3, 4, 8, 9, 10 are located at the four-point position of the main beam, and the Sections 5 and 7 are located at the position of the first boom on the left and right sides of the middle tower. As can be seen from the equipment diagram, 8 strain sensors (represented by SS, bridged to the top plate) and 2 temperature sensors (represented by TS) are arranged for each section.

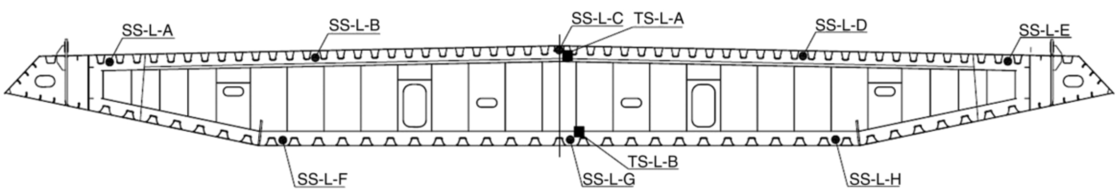


**Figure 15:** Schematic diagram of the main beam FBG sensor layout. Note: where L = 1, 2…11, corresponding to 11 steel box girder sections

### *3.7 Raw Data Analysis*

The development of health monitoring technology ensures the accuracy and reliability of fatigue life assessment of bridge structures. The strain time history data collected by the health monitoring system can reflect the actual stress and strain state of the steel box girder, which is an important basis for the fatigue sensitivity analysis of the steel box girder. For the massive data collected by the health monitoring system, how to carry out effective identification and analysis is an important prerequisite for the study of fatigue stress characteristics and health status assessment of bridge structures. This section first analyzes the raw data and finds the general rule of stress on the steel box girder, which lays the foundation for fatigue sensitivity analysis.

#### *3.7.1 Stress Time History Analysis*

The stress level of the steel box girder of Taizhou Yangtze River Bridge is low, so the strain time history obtained by the health monitoring system can be converted into the stress time course according to Hooke's law. Taking the five points of the section on January 1 and May 1 of 2013 as an example, the stress time history and the temperature time history curve are listed, as shown in Figs. 16 and 17.

It can be seen from Figs. 16 and 17 that:

1. The temperature of the top plate of the steel box girder is constantly changing. It consists of a large cycle. The temperature is the lowest at 5:00–7:00 in the morning and the highest at 15:00–17:00 at noon. The temperature change of the steel box girder roof is not only related to the temperature but also to the solar radiation. The temperature change on January 1 is relatively small (−8°C–1°C), and the temperature change on May 1 is relatively large (12°C–36°C).
2. As the temperature changes, the longitudinal bridge-to-average stress of the steel box girder also consists of a large cycle. When the temperature rises, the average stress is small, and when the temperature is lowered, the average stress is large, showing a significant negative correlation. This is caused by the thermal expansion and contraction effect of the steel box girder. When the temperature is lowered, the steel shrinks and the various parts of the steel box girder are mutually constrained, showing a large tensile stress. In the same way, the temperature rises, the average stress of the steel box

beam becomes smaller, and even the compressive stress is exhibited. At the same time, it can be seen that the magnitude of the stress change has a positive correlation with the temperature change range. Taking the measuring point SS-5-C as an example, the stress variation on January 1 is small (80 MPa–140 MPa), and the stress on May 1st The range of change is large (−40 MPa–70 MPa).

3. The average stress of the measuring point SS-5-A is the largest, the average stress of the measuring point SS-5-B is second at the same temperature, and the average stress of the measuring point SS-5-C is the smallest. This is due to the non-uniform distribution of the shear deformation of the steel box girder along the flange plate. When the box girder is bent and deformed, the longitudinal displacement of the flange plate away from the web lags behind the longitudinal displacement of the flange plate of the near web. Therefore, the longitudinal stress generated by the bending is distributed along the width of the flange plate, the stress near the web is large, and the stress away from the web is small.
4. Comparing the three strain points, there are many small mutations on the SS-5-B stress curve. This is that the SS-5-B is placed on the roof of the traffic lane and directly bears the load of the vehicle. The small sudden change is caused by the wheel pressure of the vehicle. The measuring point SS-5-A is arranged on the roof of the emergency stop belt, and the SS-5-C is arranged in the middle part of the box beam section. Generally, it is not directly affected by the wheel load, and there is almost no sudden change.

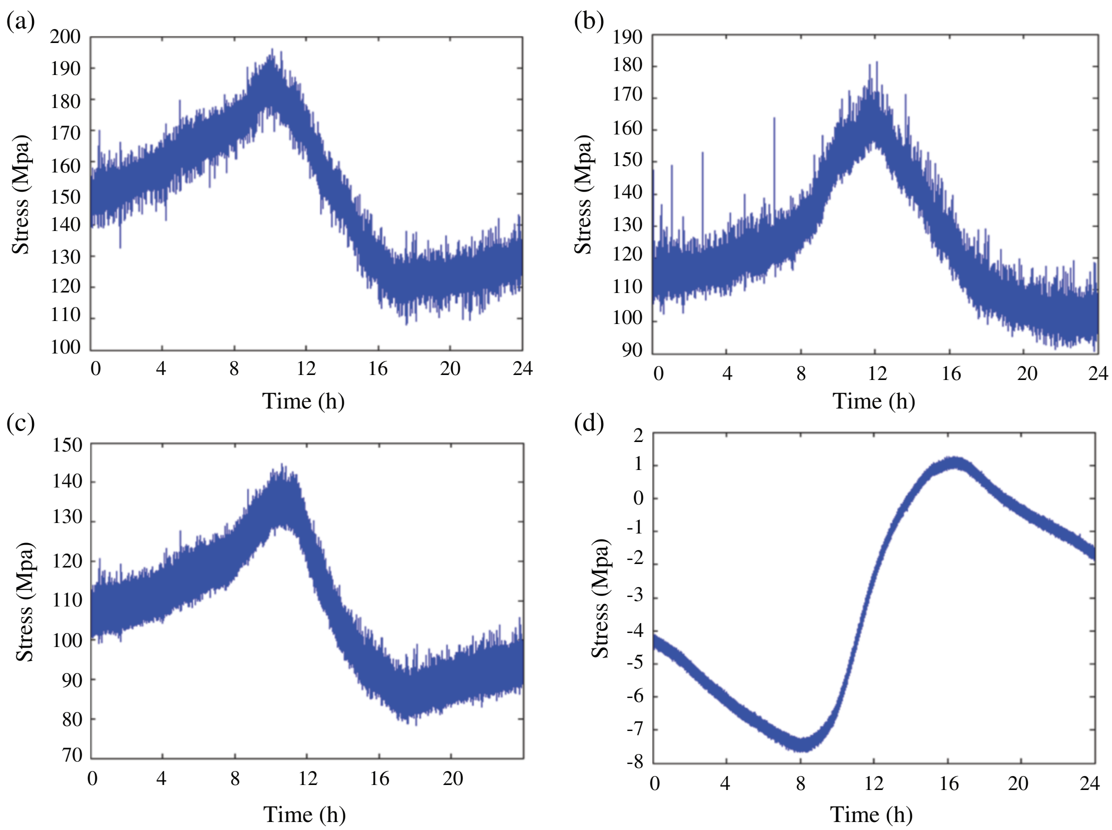


**Figure 16:** Partial measurement point stress and temperature time history curve on 2013/01/01. (a) SS-5-A stress time history curve, (b) SS-5-B stress time history curve, (c) SS-5-C stress time history curve, and (d) TS-5-A temperature time history curve

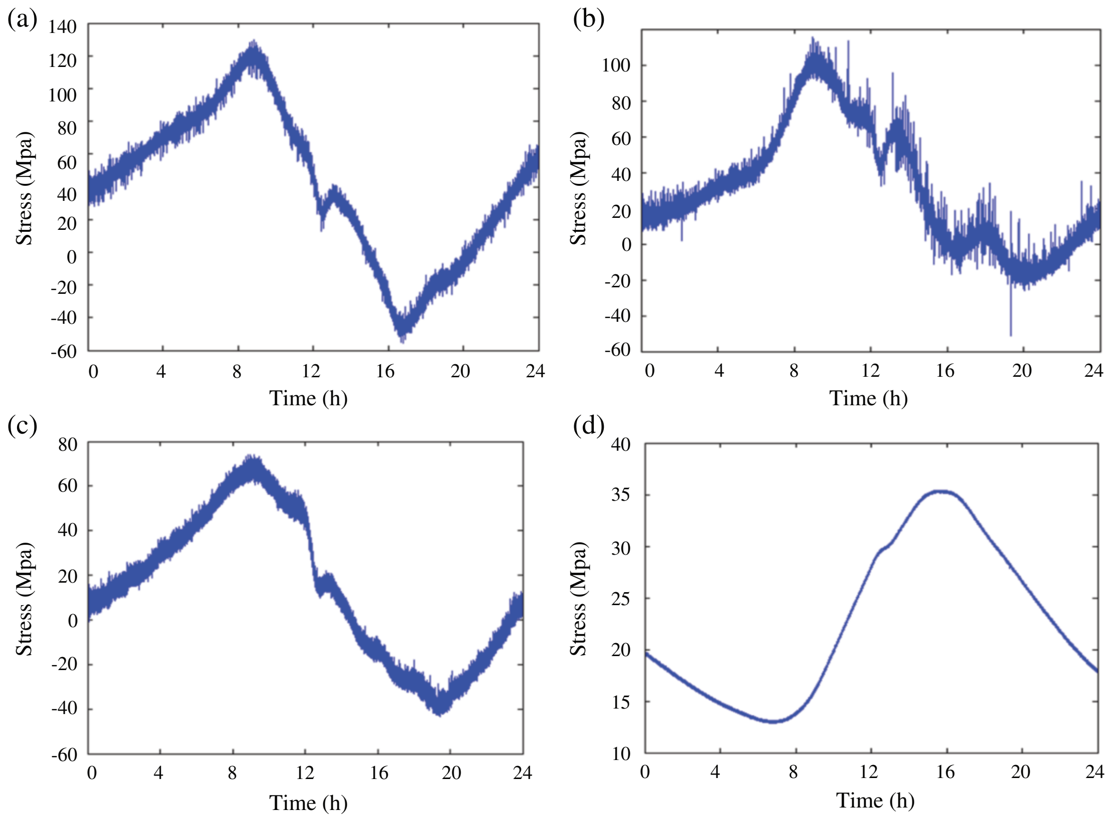


**Figure 17:** Partial measurement point stress and temperature time history curve on 2013/05/01. (a) SS-5-A stress time history curve, (b) SS-5-B stress time history curve, (c) SS-5-C stress time history curve, and (d) TS-5-A temperature time history curve

The typical stress abrupt curve of the measuring point SS-5-B is shown in Fig. 18. This mutation is caused by the direct action of the vehicle load. Each group of mutations consists of two peaks, which are caused respectively the front and rear axles of the vehicle. The front axle weight of the vehicle is less than the rear axle weight, so the stress of the first peak is less than the stress of the latter peak. The distance between the two peaks is 0.2 S in time. If the vehicle passes the bridge at 60–100 Km/h, the front and rear wheelbase of the vehicle is 3.3–5.5 m, which is consistent with the shaft spacing of most vehicles. The average width of each peak is 0.2–0.3 S, which indicates that the stress influence line of the longitudinal bridge is relatively short when the wheel load acts, so there will be multiple stress cycles when a car passes.

*3.7.2 Stress Time History Analysis*

Frequency domain processing, also called spectrum analysis, is a time-frequency transform process based on the Fourier transform. The result is a frequency-variable function called spectral function. The modulus of the spectral function is called the amplitude and is used to describe the distribution of the magnitude of the vibration with frequency.

The main statistical parameter of the frequency domain characteristics of random vibration signals is the power spectral density function. The power spectral density function of a single random vibration signal is called the self-power spectral density function. The self-power spectral density function reflects the distribution of power at each frequency of the vibration signal, allowing us to know which frequencies

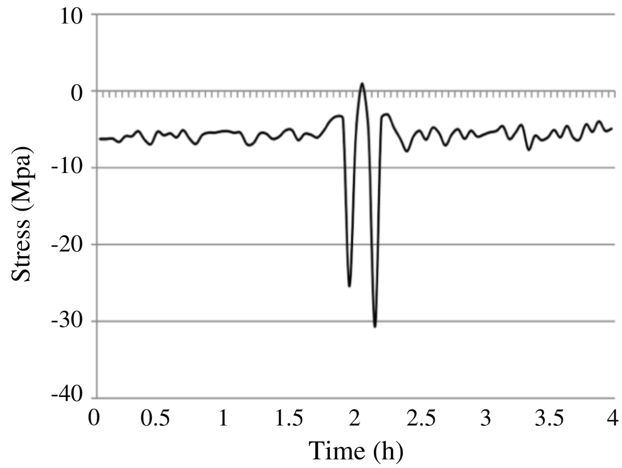


**Figure 18:** Typical stress abrupt curve

are dominant. Self-power spectra are often used to determine the natural vibration characteristics of structures or mechanical devices. In the equipment fault monitoring, the fault spectrum can be judged according to the change of the power spectrum in different time periods and the cause of the possible fault can be found. Its expression formula is:

$$Sxx(k) = \frac{1}{MN_{FFT}} \sum\nolimits_{i=1}^{M} X_i(k)X_i^*(k) \tag{12}$$

where: the Fourier transform of the $i$-th data segment of the $X_i(k)$random vibration signal, $X_i^*(k)$ is the conjugate complex number of $X_i$(k), M is the average number of times, and $N_{FFT}$ is the data length.

Taking the measurement points TS-5-A and SS-5-B on May 1, 2013 as an example, frequency domain analysis of temperature vibration signals and stress vibration signals is performed. The spectrum diagram is shown in Figs. 19 and 20. It can be seen from Fig. 19 that most of the energy of the temperature time history is distributed below 0.001 Hz. This is because the temperature changes slowly and the period is long, so the frequency is relatively low. It can be seen from Fig. 20a that most of the energy distribution of the stress time history is below 0.03 Hz. Comparing the results of temperature domain time domain frequency domain analysis, it is known that this part of energy is caused by temperature effect, sensor's own characteristics and other factors, and plays a controlling role in bridge stress and vibration data. It can be seen from Fig. 20b that there is also a partial energy distribution in the frequency domain range of 0.03–0.5 Hz. The first five-order vibration frequency of the Taizhou Bridge is located in this frequency range.The structural natural frequency component dominates the energy in this frequency band. When the frequency is greater than 0.5 Hz, the energy distribution is small, showing the characteristics of noise. Based on the structural monitoring data of the cable-stayed bridge obtained by the Donghai Bridge Health Monitoring System under the action of "Rosa" typhoon, the frequency domain analysis of the main beam was carried out with or without typhoon [22]. The analysis shows that the structural energy between 2.5 and 4.5 Hz during operation is mainly caused by traffic loads. Therefore, it can be considered that the response of the frequency range greater than 4.5 Hz is caused by noise, and the response of the frequency range between 2.5 and 4.5 Hz is caused by the vehicle crossing the bridge.

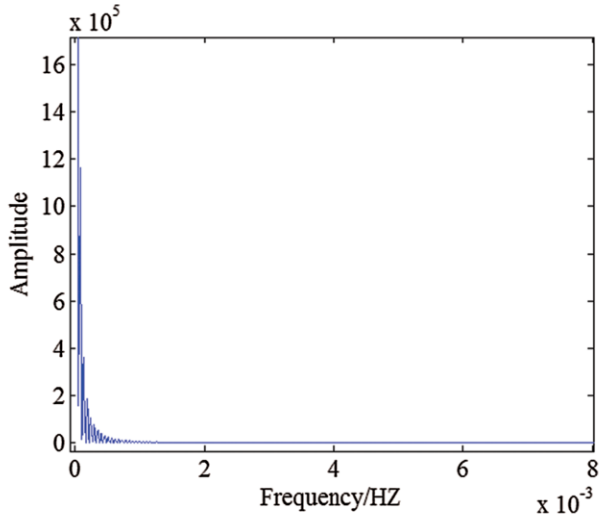


**Figure 19:** 2013/5/1 measuring point TS-5-A power spectrum

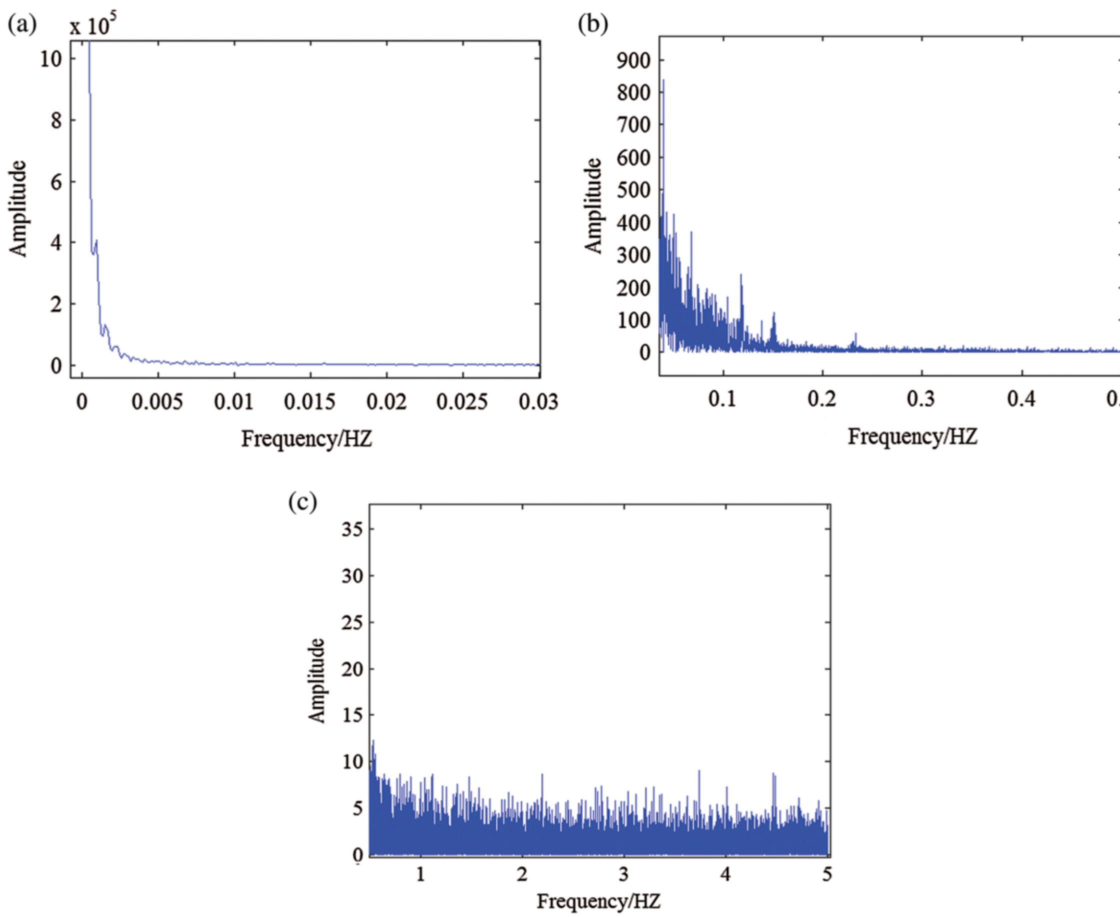


**Figure 20:** 2013/5/1 measuring point SS-5-B power spectrum. (a) 0–0.03 Hz, (b) 0.03–0.5 Hz, and (c) 0.5–5 Hz

*3.7.3 Extraction of Structural True Stress Response*

The bridge structure will be affected by environmental factors such as temperature and wind and various vehicle loads during operation, and the sampling data will be interfered by the noise signal. Therefore, the stress response collected by the bridge health monitoring system is composed of the real response of the structure, temperature deformation and random disturbance of the environment. The true response of the structure is caused by vehicle loads, which is the main cause of structural fatigue damage and the focus of structural health monitoring and condition assessment. In order to evaluate the fatigue damage of the steel box girder under the vehicle load, it is necessary to extract the stress time history data caused by the vehicle load for processing analysis.

In vibration signal analysis, digital filtering is a processing method that selects a part of the signals of interest from the collected discrete signals by mathematical operations. Its main role is to filter out noise and spurious components in the test signal, improve signal-to-noise ratio, smooth analysis data, suppress interference signals, and separate frequency components. The frequency-domain method of digital filtering is to use the FFT fast algorithm to perform discrete Fourier transform on the input signal sampling data, and analyze its spectrum. According to the filtering requirements, the frequency part that needs to be filtered is directly set to zero or the gradient transition band is set. After zeroing, the IFFT fast algorithm is used to perform the discrete Fourier transform on the filtered data to recover the time domain signal. After the signal enters the filter, some of the frequencies pass and some are blocked. The frequency range through the filter is called the pass band, and the range of frequencies that are blocked or attenuated into a small frequency band is called the stop band, and the boundary point between the pass band and the stop band is called the cutoff frequency.

In order to filter out the temperature deformation signal and noise interference in the stress time history data, and extract the true response of the structure, it is necessary to determine the cutoff frequency suitable for the monitoring data of the bridge based on the frequency domain analysis result of the stress time history data.

Since the temperature changes very slowly, it only affects the average stress of the structural members, and the average stress of the steel box girder is lower when the suspension bridge is in the bridge state, and the influence of the average stress can be neglected during the fatigue analysis, so it can be used in the fatigue analysis. The effect of the temperature effect is filtered out, that is, the data portion with a frequency less than 0.03 Hz is filtered out. Environmental noise has a great influence on fatigue assessment. Smaller disturbances may also lead to complete failure of fatigue assessment. Therefore, it is necessary to strictly control the influence of environmental noise, and directly filter out the data portion with frequency greater than 4.5 Hz. Therefore, in order to filter out the effect of temperature effect, a high-pass filter with a cutoff frequency of 0.03 Hz is designed. To filter out the interference of environmental noise, a low-pass filter with a cutoff frequency of 4.5 Hz is designed.

The stress time history data of the SS-5-B measuring point on May 1, 2013 is selected for filtering analysis, and the stress time history in various states is obtained as shown in Fig. 21. It can be seen that after the temperature stress is filtered out, the stress of the steel box girder fluctuates around 0 MPa, and the average stress is 0 MPa. After the noise is filtered out, the burr of the steel box beam is reduced, and the vibration caused by the vehicle is not significantly reduced. The bandpass filter with a minimum cutoff frequency of 0.03 Hz and a maximum cutoff frequency of 4.5 Hz can accurately extract the true response of the bridge.

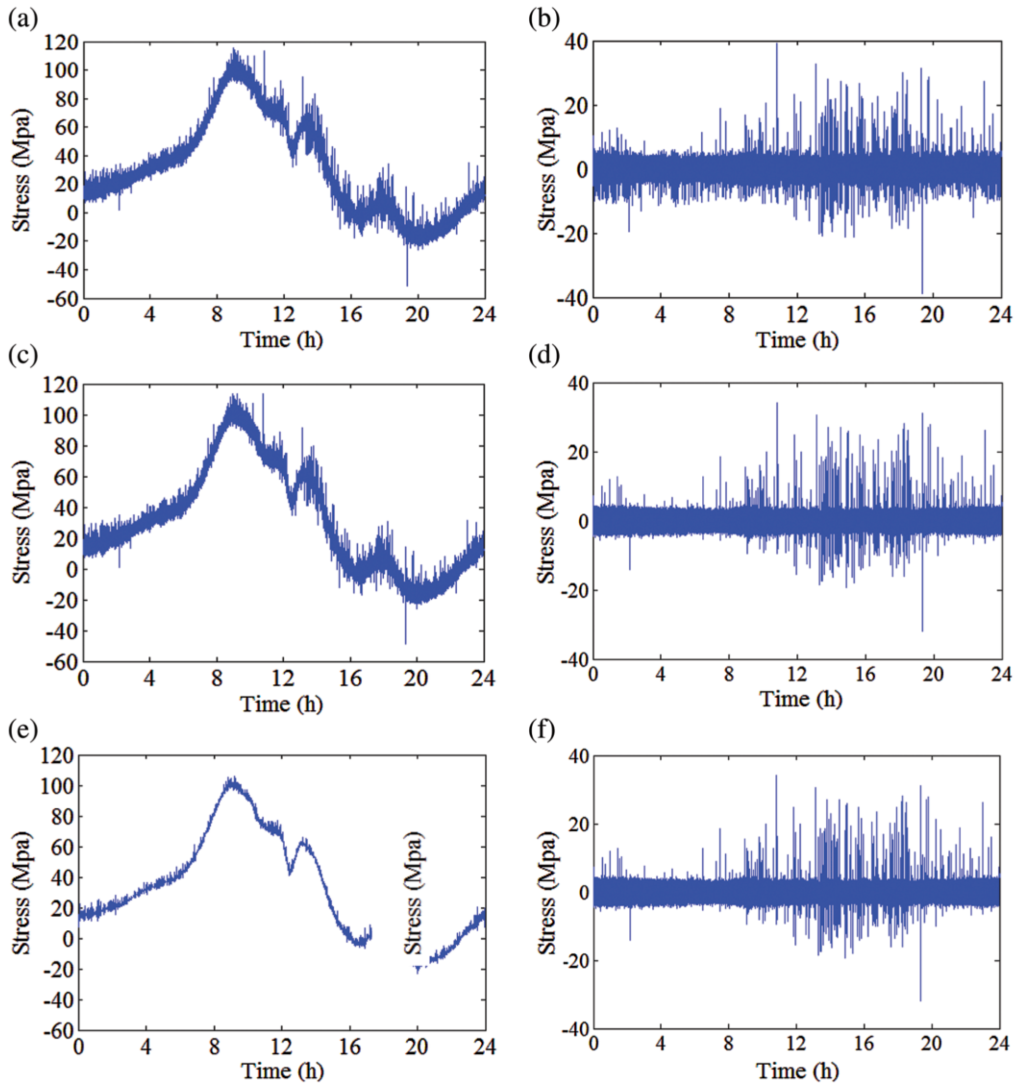


**Figure 21:** Measuring point SS-5-B filter processing. (a) Raw stress data, (b) Only filter out, (c) Only filter out noise, (d) Filter out temperature stress, (e) Temperature stress time history, and (f) Residual noise

## 4 Fatigue State Analysis and Evaluation

### *4.1 Fatigue Life Assessment Method*

The fatigue strength curve (*S-N* curve) is a curve representing the relationship between fatigue life and load stress, and is the basis for the fatigue design and fatigue evaluation of steel bridge welding details. The fatigue life assessment method based on the *S-N* curve first obtains the fatigue stress spectrum based on the stress data. On this basis, the *S-N* curve is used to obtain the damage under different stress amplitudes, and then the total damage is calculated according to a certain damage accumulation criterion, and finally the fatigue life of the detail is predicted.

In order to accurately assess the fatigue life of the bridge structure, it is necessary to fully consider the contribution of the low stress amplitude to the cumulative fatigue damage. The British BS5400 specification gives a method for dealing with low stress cycles and can relatively accurately assess the effects of low stress cycles on fatigue damage. Therefore, this paper uses the fatigue strength curve given by the specification to evaluate the fatigue life of steel box girder. The fatigue strength curves specified in the BS5400 specification are briefly described below.

The BS5400 specification classifies the fatigue details of steel bridges into nine categories, as shown in Tab. 6. The *S-N* curve is:

$$\mathrm{N} \times S_r^m = K_2 \quad (\mathrm{N} \le 10^7) \tag{13}$$

$$\mathrm{N} \times S_r^{m+2} = K_2 S_0^2 \quad (\mathrm{N} > 10^7) \tag{14}$$

$$K_2 = K_0 \times \Delta^2 \tag{15}$$

In the formula, $m$ represents the inverse slope of the lg $N$ and lg $S_r$ curves, and generally takes a value of 3. $S_r$ represents the stress amplitude, and $N$ represents the number of cycles corresponding thereto. $S_0$ represents the corresponding stress amplitude when the fatigue life is 1 × $10^7$ times. It can be seen that the curve considers the effect of all stress cycles on the fatigue life assessment, but the slope of the *S-N* curve exceeding the stress cycle of 1 × $10^7$ times should change from $m$ to $m$ + 2. $K_2$ represents the fatigue strength coefficient when the probability of surpass is 2.3%.

**Table 6:** Fatigue details of BS5400 specification *S-N* curve parameters

| Classification | W | G | F2 | F | E | D | C | B | S |
|---|---|---|---|---|---|---|---|---|---|
| $K_0$ | 0.37 × $10^{12}$ | 0.57 × $10^{12}$ | 1.32 × $10^{12}$ | 1.73 × $10^{12}$ | 3.29 × $10^{12}$ | 3.99 × $10^{12}$ | 1.08 × $10^{12}$ | 2.34 × $10^{12}$ | 2.13 × $10^{12}$ |
| Δ | 0.654 | 0.662 | 0.592 | 0.605 | 0.561 | 0.617 | 0.625 | 0.657 | 0.313 |
| $m$ | 3 | 3 | 3 | 3 | 3 | 3 | 3.5 | 4 | 4 |

### *4.2 Fatigue Damage Accumulation Calculation Method*

The fatigue problem of steel bridge structure has the characteristics of variable amplitude and long life. It is necessary to study the fatigue performance of steel bridge under variable amplitude fatigue load, so the theory of fatigue damage accumulation is introduced. The most widely used method is the Miner linear damage accumulation theory. It is considered that fatigue damage is a linear superposition of fatigue damage caused by each variable amplitude stress cycle $S_i$. The expression is as follows:

$$D = \frac{n_1}{N_1} + \frac{n_2}{N_2} + \ldots + \frac{n_n}{N_n} = \sum_{i=1}^{n} \frac{n_i}{N_i} \tag{16}$$

In the formula, $n_i$ is the number of times of stress cycle $S_i$, and $N_i$ is the fatigue life of stress cycle $S_i$ in the constant amplitude *S-N* curve. The Miner criterion states that the fatigue damage condition is $D \ge 1$.

Based on the fatigue strength curve of BS5400 specification, considering the effects of high stress cycle and low stress cycle, the fatigue damage caused by stress cycle $S$ is:

$$D_s = \frac{n}{N} = \frac{nS^3}{K_2} \quad (S \ge S_0) \tag{17}$$

$$D_s = \frac{n}{N} = \frac{nS^5}{K_2 S_0^2} \quad (S < S_0) \tag{18}$$

According to the Miner linear damage accumulation theory, the fatigue damage of the detail under the variable amplitude load is:

$$D = \sum_{S_i \geq S_0} \frac{n_i S_i^3}{K_2} + \sum_{S_j < S_0} \frac{n_j S_j^5}{K_2 S_0^2} \tag{19}$$

In formula $n_i$ and $n_j$, respectively, denote the number of stress cycles greater than or equal to $S_0$ or less than $S_0$.

### *4.3 Stress Amplitude Spectrum Analysis*

Fatigue analysis was carried out on the stress time-history data obtained from the SS-5-B and SS-5-C measuring points on May 1, 2013. The stress time-history data under the vehicle load was extracted and the rain flow analysis was performed to obtain the stress amplitude. The values are shown in Tabs. 7 and 8. Since the Taizhou Yangtze River Bridge is in the open-air phase, the stress amplitude on the bridge is very small, the maximum value is 34 MPa, and the fatigue limit is not reached. However, the contribution of these smaller stress amplitudes smaller than the fatigue limit to fatigue damage cannot be ignored.

**Table 7:** SS-5-B stress amplitude spectrum

| Stress amplitude (MPa) | ≤4 | 4-6 | 6-8 | 8-10 | 10-12 | 12-14 | 14-16 | 16-18 | 18-20 | 20-22 | 22-24 | 24-26 | 26-28 | 28-30 | 30-32 | 32-34 |
|---|---|---|---|---|---|---|---|---|---|---|---|---|---|---|---|---|
| Cycle Number | 1900 | 286 | 72 | 45 | 25 | 19 | 17 | 12 | 7 | 3 | 3 | 2 | 0 | 1 | 0 | 1 |

**Table 8:** SS-5-C stress amplitude spectrum

| Stress amplitude (MPa) | ≤4 | 4-6 | 6-8 | 8-10 | 10-12 | 12-14 | 14-16 | 16-18 | 18-20 | 20-22 | 22-24 | 24-26 | 26-28 | 28-30 | 30-32 | 32-34 |
|---|---|---|---|---|---|---|---|---|---|---|---|---|---|---|---|---|
| Cycle Number | 2310 | 311 | 0 | 0 | 0 | 0 | 0 | 0 | 0 | 0 | 0 | 0 | 0 | 0 | 0 | 0 |

Since the steel box girder at the measuring point SS-5-C is not directly subjected to the direct load of the vehicle load, the stress amplitude is within 6 MPa. These stress cycles are caused by the self-vibration of the bridge. The steel box girder at the measuring point SS-5-B is located in the fast lane and directly bears the load of the vehicle. The number of cycles of the stress amplitude in the range of 6 MPa–34 MPa reaches 207 times. These stress cycles are caused by the vehicle load. At the same time, the number of cycles with a stress amplitude of less than 6 MPa has reached 2,186 times, occupying most of the stress cycle. This part of the stress cycle is not caused by the direct action of the vehicle load, so it can be ignored.

In order to visually display the fatigue state of the steel box girder under different vehicle loads under different vehicle sections, the stress time-history data collected by the fast track position measuring point (SS-LB) of each section on May 1, 2013 is filtered to carry out the rain flow analysis. The calculation results are shown in Tab. 9. It can be seen from that the low amplitude stress cycle of each measuring point occupies most of the stress cycle, and the number of stress cycles less than 6 MPa is about 2000 times. These small stress cycles are caused by the self-vibration of the bridge and are not the result of the vehicle load. They are negligible in the fatigue analysis under vehicle load. As the stress amplitude increases, the number of stress cycles decreases. These relatively high stress cycles are caused by the direct action of vehicle loads and are the direct cause of fatigue damage of steel box girder.

**Table 9:** Stress amplitude spectrum of each section

| Cycle number | Stress amplitude (MPa) | | | | | | | |
|---|---|---|---|---|---|---|---|---|
| | 0-6 | 6-10 | 10-15 | 15-20 | 20-25 | 25-30 | 30-35 | 35-40 |
| SS-1-B | 2394 | 143 | 21 | 9 | 8 | 0 | 0 | 0 |
| SS-2-B | 2008 | 123 | 37 | 13 | 2 | 3 | 0 | 0 |
| SS-3-B | 1998 | 133 | 15 | 9 | 2 | 2 | 2 | 0 |
| SS-4-B | 2359 | 189 | 34 | 20 | 7 | 3 | 1 | 0 |
| SS-5-B | 2186 | 185 | 53 | 27 | 7 | 2 | 1 | 0 |
| SS-6-B | 2456 | 88 | 22 | 7 | 3 | 0 | 1 | 0 |
| SS-7-B | 1938 | 169 | 18 | 14 | 11 | 0 | 0 | 3 |
| SS-8-B | 2101 | 348 | 81 | 30 | 13 | 3 | 1 | 0 |
| SS-9-B | 2053 | 114 | 17 | 13 | 1 | 1 | 0 | 0 |
| SS-10-B | 2374 | 190 | 56 | 18 | 11 | 2 | 3 | 1 |
| SS-11-B | 2462 | 279 | 46 | 18 | 7 | 3 | 3 | 0 |

### *4.4 Incremental Analysis of Fatigue Damage*

For large-span bridges, there are many kinds of vehicles operating on the bridge deck. The landing area and wheel load weight of different wheels are also different. Therefore, the magnitude of fatigue stress caused by different vehicles crossing bridges is also different. At the same time, the Taizhou Yangtze Bridge is in the open-air phase, and the stress amplitude obtained by the sensor has not reached the threshold value of fatigue damage. The fatigue damage value itself is very small, and it is impossible to accurately measure the fatigue state of the bridge. Therefore, this paper uses the daily fatigue damage increment to measure the fatigue sensitivity of each section.

The foregoing analysis shows that the ambient temperature directly determines the average stress of the steel box girder. Therefore, this section uses the ambient temperature as a reference for representative multi-days (2013-1-1, 2013-4-1, 2013-5-1, 2013-5-7, 2013-8-1, 2013-10- 1, 2013-10-7) Investigate the stress time history, and use the method described in Section 3.4.1 to obtain the fatigue damage increments of each daily measurement point (SS-LB) as shown in Tab. 10. It can be seen that the fatigue damage increments of each

**Table 10:** Multi-day damage increment of each measuring point

| Date | Test section | | | | | | | | | | |
|---|---|---|---|---|---|---|---|---|---|---|---|
| | 1 | 2 | 3 | 4 | 5 | 6 | 7 | 8 | 9 | 10 | 11 |
| 2013-1-1 | 1.02 | 6.43 | 4.76 | 3.89 | 7.11 | 3.82 | 7.20 | 6.23 | 1.25 | 8.81 | 3.25 |
| 2013-4-1 | 2.76 | 2.98 | 1.66 | 2.24 | 6.30 | 7.20 | 3.93 | 2.57 | 9.17 | 2.09 | 1.45 |
| 2013-5-1 | 3.87 | 3.60 | 2.94 | 4.99 | 3.46 | 1.37 | 3.23 | 1.37 | 7.38 | 5.76 | 4.85 |
| 2013-5-7 | 2.08 | 5.69 | 8.25 | 2.03 | 6.72 | 7.73 | 9.52 | 2.16 | 1.49 | 3.37 | 1.23 |
| 2013-8-1 | 5.10 | 2.46 | 2.17 | 7.10 | 9.55 | 5.01 | 3.05 | 1.21 | 2.35 | 7.69 | 7.51 |
| 2013-10-1 | 4.36 | 2.11 | 2.34 | 4.48 | 6.34 | 5.65 | 6.86 | 2.87 | 8.50 | 2.35 | 3.64 |
| 2013-10-7 | 3.58 | 2.36 | 2.09 | 2.48 | 6.20 | 7.31 | 7.36 | 5.63 | 9.94 | 3.31 | 2.66 |

measuring point are different in the same day, so the stress response of the steel box girder under the load of the vehicle is different at each measuring point. The fatigue damage increment can accurately estimate the fatigue state of the structure and can be used as an evaluation index for fatigue sensitivity analysis.

The same measurement points have different increments of fatigue damage on each day, and there is a large dispersion, which is caused by the difference in daily traffic load flow. In previous studies, the traffic flow spectrum survey based on one day was generally used as a traffic flow for a period of time, or by investigating the strain data collected by the health monitoring system for one day as a representative stress time period. Fatigue analysis with only one day or one week of data does not accurately reflect the true fatigue state of the bridge. Therefore, it is necessary to investigate the stress time-history data of many days, and obtain the daily average cumulative damage increment value of different sections of the steel box girder structure to determine the fatigue critical section of the steel box girder.

A sample of 122 days of health monitoring data for the Taizhou Bridge for 4 months (April 2013-July 2013) was investigated. After filtering the daily stress time history, the rain flow counting process is performed to obtain the daily stress amplitude, and then the daily fatigue damage increment is calculated. After averaging, the daily average fatigue damage increment can be obtained, as shown in Tab. 11. It can be seen that the daily average fatigue damage increment of steel box girder with different sections under vehicle load is about the same, with an average of $3.1 \times 10^{-7}$. Since the Taizhou Bridge is in the open-air phase, the stress amplitude obtained by the sensor has not reached the threshold of fatigue damage, so the fatigue damage value is very small. The daily average fatigue damage increment of Section 5 and Section 7 (as shown in Fig. 15) is relatively large, more than 10% above the average. Under the same operating traffic flow, these two parts will be damaged before other parts. That is to say, the beam section near the steel tower, especially the beam section at the position of the first boom around the middle tower is relatively obvious, which is the key section for fatigue analysis, which is consistent with the calculation results of FEM.

**Table 11:** Daily average fatigue damage increment of each measuring point

| Test section | 1 | 2 | 3 | 4 | 5 | 6 | 7 | 8 | 9 | 10 | 11 |
|---|---|---|---|---|---|---|---|---|---|---|---|
| Fatigue damage increment ($\times 10^{-7}$) | 3.02 | 2.69 | 3.18 | 3.22 | 3.54 | 3.15 | 3.43 | 2.85 | 3.10 | 3.12 | 2.78 |
| Rate of change (%) | −2.52 | −13.1 | 2.64 | 3.93 | 14.23 | 1.67 | 10.7 | −8.01 | 0.06 | 0.70 | −10.3 |

## 5 Conclusions

1. Using the beam4 element to simulate the main beam to establish the “spine beam” model of the Taizhou Yangtze River Bridge, the calculated low-order vibration mode frequency of the structure is in good agreement with the completion test results. The model can simulate the overall dynamic response of the bridge.
2. The fundamental frequency of Taizhou Yangtze River Bridge is 0.08443 Hz, which has a long structural period and has obvious large-span flexible structural features. However, due to the restraint of the middle tower, the vibration mode is quite different from that of the two tower suspension bridge.
3. Under the action of random traffic flow, the vertical displacement response of the Taizhou Yangtze River Bridge is the largest, the maximum value is 1.01 m, and the vertical displacement response of the steel box girder at the corresponding section position is approximately the same. However, the vertical displacement response of the same main span at the corresponding section position is different, and the displacement response of the tower beam section near the steel is larger than that of the side tower section.

4. The stress amplitude on the bridge is mainly caused by the vehicle load. The temperature only affects the average stress of the structure, and the noise will have a greater impact on the fatigue assessment. In the fatigue analysis under vehicle load, the effects of temperature and noise should be filtered out to extract the true response of the structure under vehicle load.
5. Most of the energy of the stress time history is distributed in the frequency range below 0.03 Hz. This part of the energy is caused by temperature effects and the characteristics of the sensor itself. The structural energy in the frequency range between 2.5 and 4.5 Hz during operation is mainly caused by traffic loads. A bandpass filter with a minimum cutoff frequency of 0.03 Hz and a maximum cutoff frequency of 4.5 Hz can relatively accurately extract the true response of the bridge.
6. The fatigue effect of the beam section near the steel tower, especially the first section of the middle tower, is the key section of the fatigue analysis by health morning system, which is consistent with the calculation results of FEM.

**Funding Statement:** This research has been supported by the National Natural Science Foundation of China (Grant No. 51778135), the National Key R&D Program Foundation of China (Grant No. 2017YFC0806001), the Natural Science Foundation of Jiangsu Province, China (Grant No. BK20160207), and Aeronautical Science Foundation of China (Grant No. 20130969010), the Fundamental Research Funds for the Central Universities and Postgraduate Research & Practice Innovation Program of Jiangsu Province, China (Grant No. KYCX18_0113 and KYLX16_0253). This research also has been supported by China Scholarship Council.

**Conflicts of Interest:** The authors declare that they have no conflicts of interest to report regarding the present study.

**References**

1. Wu, C., Yuan, Y., Jiang, X. (2016). Fatigue behavior assessment method of the orthotropic steel deck for a self-anchored suspension railway bridge. *Procedia Engineering, 161,* 91–96. DOI 10.1016/j.proeng.2016.08.503.
2. Yang, M. Y., Kainuma, S., Jeong, Y. S. (2018). Structural behavior of orthotropic steel decks with artificial cracks in longitudinal ribs. *Journal of Constructional Steel Research, 141,* 132–144. DOI 10.1016/j.jcsr.2017.11.007.
3. Deng, Y., Li, A. Q., Feng, D. M. (2018). Fatigue reliability assessment for orthotropic steel decks based on long term strain monitoring. *Sensors, 18(1),* 181. DOI 10.3390/s18010181.
4. Farrar, C. R., James, G. H. (1997). System identification from ambient vibration measurements on bridges. *Journal of Sound and Vibration, 205(1),* 1–18. DOI 10.1006/jsvi.1997.0977.
5. Seo, J., Hu, J., Lee, J. (2016). Summary review of structural health monitoring applications for highway bridges. *Journal of Performance of Constructed Facilities, 30(4),* 4015072. DOI 10.1061/(ASCE)CF.1943-5509.0000824.
6. Wenzel, H. (2009). *Health monitoring of bridges*. New York: John Wiley & Sons, Inc.
7. Sousa, H., Félix, C., Bento, J., Figueiras, J. (2011). Design and implementation of a monitoring system applied to a long-span prestressed concrete bridge. *Structural Concrete, 12(2),* 82–93. DOI 10.1002/suco.201000014.
8. Sousa, H., Cavadas, F., Henriques, A., Bento, J., Figueiras, J. (2013). Bridge deflection evaluation using strain and rotation measurements. *Smart Structures and Systems, 11(4),* 365–386. DOI 10.12989/sss.2013.11.4.365.
9. Sousa, H., Costa, B., Henriques, A., Bento, J., Figueiras, J. (2016). Assessment of traffic load events and structural effects on road bridges based on strain measurements. *Journal of Civil Engineering and Management, 22(4),* 457–469. DOI 10.3846/13923730.2014.897991.
10. Hodgson, I. (2007). *Personal discussion for the acquisition of the real data from the monitoring of the I-39 Northbound Bridge over the Wisconsin River*. Ian Hodgson, Senior Research Engineer. Department of Civil and Environmental Engineering. ATLSS Center. Lehigh University 117 ATLSS Dr. Bethlehem.
11. Frangopol, D. M., Strauss, A., Kim, S. (2008). Use of monitoring extreme data for the performance prediction of structures: general approach. *Engineering Structures, 30(12),* 3644–3653.

12. Kainuma, S., Yang, M., Jeong, Y. S., Inokuchi, S., Kawabata, A. et al. (2016). Experiment on fatigue behavior of rib-to-deck weld root in orthotropic steel decks. *Journal of Constructional Steel Research, 119,* 113–122. DOI 10.1016/j.jcsr.2015.11.014.
13. Zhang, Q. H., Bu, Y. Z., Qiao, L. I. (2017). Review on fatigue problems of orthotropic steel bridge deck. *China Journal of Highway & Transport, 30(3),* 14–30 and 39.
14. Connor, R., Fisher, J., Gatti, W., Gopalaratnam, V., Kozy, B. et al. (2012). *Manual for Design, Construction, and Maintenance of Orthotropic Steel Deck Bridges*. Report No. FHWA-IF-12-027, Washington, DC: Federal Highway Administration.
15. Wang, G., Ding, Y., Song, Y., Wei, Z. (2016). Influence of temperature action on the fatigue effect of steel deck with pavement. *Engineering Mechanics, 33(5),* 115–123.
16. Heng, J., Zheng, K., Gou, C., Zhang, Y., Bao, Y. (2017). Fatigue performance of rib-to-deck joints in orthotropic steel decks with thickened edge u-ribs. *Journal of Bridge Engineering, 22(9),* 04017059. DOI 10.1061/(ASCE) BE.1943-5592.0001095.
17. Fu, Z., Ji, B., Zhang, C., Wang, Q. (2017). Fatigue performance of roof and U-rib weld of orthotropic steel bridge deck with different penetration rates. *Journal of Bridge Engineering, 22(6),* 04017016. DOI 10.1061/(ASCE) BE.1943-5592.0001036.
18. Fu, Z., Ji, B., Zhang, C., Li, D. (2018). Experimental study on the fatigue performance of roof and U-rib welds of orthotropic steel bridge decks. *KSCE Journal of Civil Engineering, 22(1),* 270–278. DOI 10.1007/s12205-017-1725-0.
19. Lu, N. W., Liu, Y., Deng, Y. (2019). Fatigue reliability evaluation of orthotropic steel bridge decks based on site-specific weigh-in-motion measurements. *International Journal of Steel Structures, 19(1),* 181–192. DOI 10.1007/s13296-018-0109-8.
20. Alamdar, M. M., Rakotoarivelo, T., Khoa, N. L. D. (2017). A spectral-based clustering for structural health monitoring of the Sydney Harbour Bridge. *Mechanical Systems and Signal Processing, 87,* 384–400. DOI 10.1016/j.ymssp.2016.10.033.
21. Rubinstein, R. Y., Kroese, D. P. (1981). *Simulation and the Monte Carlo Method*. *Wiley Series in Probability and Mathematical Statistics*. New York: John Wiley & Sons, Inc.
22. Min, Z. H., Sun, Z. H., Dan, D. H. (2009). Analysis of wind-induced response and dynamic properties of cable-stayed bridge under typhoon. *Journal of Tongji University (Natural Science), 37(9),* 1139–1145,1173. DOI 10.3969/j.issn.0253-374x.2009.09.001.